

LoCuSS: the connection between brightest cluster galaxy activity, gas cooling and dynamical disturbance of X-ray cluster cores

Alastair J. R. Sanderson,^{*}¹ Alastair C. Edge² and Graham P. Smith¹

¹*School of Physics and Astronomy, University of Birmingham, Edgbaston, Birmingham B15 2TT, UK*

²*Institute for Computational Cosmology, Department of Physics, University of Durham, South Road, Durham DH1 3LE*

Accepted 2009 June 8. Received 2009 June 8; in original form 2009 March 27 (*svn Revision* : 77)

ABSTRACT

We study the distribution of projected offsets between the cluster X-ray centroid and the brightest cluster galaxy (BCG) for 65 X-ray selected clusters from the Local Cluster Substructure Survey (LoCuSS), with a median redshift of $z = 0.23$. We find a clear correlation between X-ray/BCG projected offset and the logarithmic slope of the cluster gas density profile at $0.04r_{500}$ (α), implying that more dynamically disturbed clusters have weaker cool cores. Furthermore, there is a close correspondence between the activity of the BCG, in terms of detected H α and radio emission, and the X-ray/BCG offset, with the line emitting galaxies all residing in clusters with X-ray/BCG offsets of ≤ 15 kpc. Of the BCGs with $\alpha < -0.85$ and an offset $< 0.02r_{500}$, 96 per cent (23/24) have optical emission and 88 per cent (21/24) are radio active, while none has optical emission outside these criteria. We also study the cluster gas fraction (f_{gas}) within r_{500} and find a significant correlation with X-ray/BCG projected offset. The mean f_{gas} of the ‘small offset’ clusters ($< 0.02r_{500}$) is 0.106 ± 0.005 ($\sigma = 0.03$) compared to 0.145 ± 0.009 ($\sigma = 0.04$) for those with an offset $> 0.02r_{500}$, indicating that the total mass may be systematically underestimated in clusters with larger X-ray/BCG offsets. Our results imply a link between cool core strength and cluster dynamical state consistent with the view that cluster mergers can significantly perturb cool cores, and set new constraints on models of the evolution of the intracluster medium.

Key words: galaxies: clusters: general – X-rays: galaxies clusters – cooling flows – galaxies: evolution – galaxies: elliptical and lenticular, cD

1 INTRODUCTION

The first ranked, or brightest cluster galaxies (BCGs) are amongst the brightest of all galaxies, accounting for around 5–10 per cent of the total light in massive clusters (Lin & Mohr 2004). Their properties are closely related to those of the host cluster (Edge 1991; Lin & Mohr 2004) and they typically lie at the bottom of the potential well. In relaxed clusters, this location is frequently positioned within a ‘cool core’ in the intracluster medium (ICM), where gas is capable of condensing out of the hot phase, to form stars (e.g. Crawford et al. 1999; Rafferty, McNamara & Nulsen 2008) or fuel accretion onto a central supermassive black hole (e.g. Best et al. 2007). In this configuration the BCG lies at a interface which is crucial to understanding the role of feedback in galaxy and cluster evolution.

The unique character of BCGs allows them to be used as important diagnostics of the host cluster. In particular, the projected offset between the X-ray peak and the BCG is sensitive to the cluster dynamical state (Katayama et al. 2003), which is

analogous to the offset between the peaks of the gravitational lensing mass map and the X-ray emission as an indicator of disturbance (Smith et al. 2005). Furthermore, the presence of H α emission from ongoing star formation (e.g. Heckman 1981; Peres et al. 1998; Crawford et al. 1999; Edwards et al. 2007; Cavagnolo et al. 2008) and radio emission from active galactic nuclei (AGN) activity (e.g. Peres et al. 1998; Best et al. 2007; Cavagnolo et al. 2008; Mittal et al. 2008) probe the thermodynamic state of the hot gas in the cluster core. For example, it has recently been discovered that star formation in BCGs only occurs when the entropy of the ICM falls below a critical threshold (Voit et al. 2008; Rafferty et al. 2008). Moreover, almost all clusters with star-forming BCGs lie above the X-ray luminosity-temperature relation (Bildfell et al. 2008), demonstrating the close link between the BCG and global cluster properties.

With the advent of *Chandra* it is possible to probe cluster gas properties on the scale of BCGs out to intermediate redshifts and with its extensive archive of observations, this type of analysis can be applied to large numbers of clusters. In this paper we use *Chandra* data to explore the connection between cooling in cluster cores and the location and activity of the BCG for an X-

* E-mail: ajrs@star.sr.bham.ac.uk

ray selected sample of 65 clusters drawn from the Local Cluster Substructure Survey¹ (LoCuSS). This is a morphologically unbiased sample of ~ 100 X-ray luminous galaxy clusters selected from the (e)BCS and REFLEX ROSAT All Sky Survey (RASS) catalogues (e.g. see Zhang et al. 2008; Okabe et al. 2009), containing all clusters down to the RASS flux limit, within the LoCuSS redshift, declination and Galactic column cuts. Throughout this paper we assume $H_0 = 70 \text{ km s}^{-1} \text{ Mpc}^{-1}$, $\Omega_m = 0.3$ and $\Omega_\Lambda = 0.7$. Errors are quoted at a 68 per cent confidence level.

2 SAMPLE SELECTION AND DATA ANALYSIS

We select all clusters with available Chandra data that satisfy the LoCuSS selection function of $0.15 \leq z \leq 0.3$, $-70^\circ \leq \delta \leq 70^\circ$, $n_H < 7 \times 10^{20} \text{ cm}^{-2}$. This produces a total of 66 clusters, from which we discard ZwCl 1309.1+2216 because the data on this cluster are too shallow for our purposes. The median redshift is $z = 0.23$ with a corresponding scale factor of 3.7 kpc per arcsecond. Eighteen of the 65 cluster observations are drawn from our own Chandra programs in Cycles 9 and 10 (PIDs: 09800732, 10800565), the remaining observations are from the archive.

2.1 X-ray data analysis

Chandra data were reduced and analysed according to the procedure described in Sanderson, O’Sullivan & Ponman (2009). Briefly, the Chandra data were reprocessed using CIAO version 3.4 and incorporating CALDB version 3.4.2, to produce flare cleaned and point source removed level 2 events files. Corresponding blank sky background datasets were also produced and matched in normalization to the cluster events in each case, to account for variations in the particle-dominated high energy background. No adjustment was made to the background to allow for any variation in soft Galactic foreground emission compared to each cluster observation. However, following Sanderson, Ponman & O’Sullivan (2006), the galactic absorbing column was fitted as a free parameter in the spectral modelling to allow for any differences in inferred low energy absorption associated with soft emission excesses or calibration uncertainties. For some clusters, it was necessary to freeze the absorbing column at the galactic HI value, since unfeasibly low values were otherwise obtained in many of the annular bins.

A series of annular spectra were extracted for each cluster, comprising between 6 and 25 radial bins in total, depending on data quality. These annular spectra were then fitted with an absorbed APEC model using the PROJCT scheme in XSPEC version 11.3.2 to yield deprojected gas temperature and density profiles for each cluster. Weighted response matrix files were used for each spectrum, and the fitting was performed in the energy range 0.5–7.0 keV. In order to provide more reliable error estimates on the annular spectral measurements, we performed 200 Poisson realizations of the best-fit PROJCT model, using the same background and response files (Sanderson, in preparation). Each realization was treated like the original data and fitted with the PROJCT scheme to produce a suite of simulated measurements in each bin. The errors in each bin were then calculated from the median absolute deviation of these simulated values, as a robust estimator of the standard deviation that is well-suited to heavy-tailed distributions (see Beers, Flynn & Gebhardt 1990, for example).

We note that a potential issue with our Chandra analysis is the possibility of a modest bias in temperature estimates for hotter clusters ($\gtrsim 4\text{--}5 \text{ keV}$) resulting from errors in the Chandra response matrix (as described in Sun et al. 2009, and references therein), which could lead to overestimates of the temperature. To assess the magnitude of the effect this could have on our analysis, we have reanalysed one of the cluster datasets using CIAO version 4.1, incorporating CALDB version 4.1.2. We have selected Abell 1835 (obsid 6880), since this is a deep observation (120 ks) of a bright, massive cluster, where the impact of calibration changes is likely to be greatest. Using the new calibration data, we find that r_{500} changes to $1432 \pm 60 \text{ kpc}$ (from 1506 ± 57 , in our original analysis), with a corresponding gas fraction within r_{500} of 0.128 ± 0.011 (0.110 ± 0.008 originally). As expected, the newer CALDB results in a lower r_{500} and hence higher gas fraction (due to both a systematic lowering of the temperature leading to a lower total mass, as well as an increase in the gas mass measured from the emissivity), but the effect is only ~ 5 per cent for r_{500} and 16 per cent for the gas fraction; corresponding to 1.2 and 1.6σ , respectively. Since only two of our clusters are cooler than 4 keV, such a systematic shift will be similar across the whole sample and so is not likely to impact our results significantly.

The centroid for the spectral profile analysis was used to determine the projected offset between the centre of the cluster X-ray halo and the BCG. We determined this position in a similar fashion to Maughan et al. (2008), iteratively refining the cluster X-ray surface brightness centroid within an aperture of 2–3 arcmin initially, then repeating the centroiding within an aperture of ~ 1 arcmin. In addition, we also determined the coordinates of the X-ray peak as an alternative reference position to compare with the BCG location (see Section 4.1). To minimize the impact of Poisson noise, we constructed a smoothed 0.5–2.0 keV image for each cluster using the wavelet decomposition method of Vikhlinin et al. (1998). The X-ray peak was determined as the highest pixel nearest to the X-ray centroid, ignoring any non-cluster point sources, which were identified by being detected on only the smallest 1–2 wavelet scales. We have neglected the (small) uncertainty in the measurement of the X-ray centroid and peak, and therefore also in the corresponding projected distance to the BCG, since this is insignificant compared to the uncertainties on other parameters.

2.2 BCG identification and properties

The positions of the BCG optical peaks were obtained from several sources: near-infrared imaging from the Hale 200-in telescope at Palomar Observatory², described in detail in Stott et al. (2008); near-infrared data from the CTIO 4-m telescope³ (Hamilton-Morris et al., in preparation); optical imaging from VLT/FORS2⁴ (PI Edge), as well as the Digitized Sky Survey. Photometry of these imaging data were supplemented by spectroscopic confirmation of membership, using spectra from several sources (see below). The BCG was identified as the brightest galaxy in the central few hundred kpc of the cluster. In a few cases the BCG could not be identified unambiguously, but these appear to be merging clusters in

¹ <http://www.sr.bham.ac.uk/locuss>

² The Hale Telescope at Palomar Observatory is owned and operated by the California Institute of Technology.

³ Operated by the Association of Universities for Research in Astronomy Inc.

⁴ Operated by the European Southern Observatory

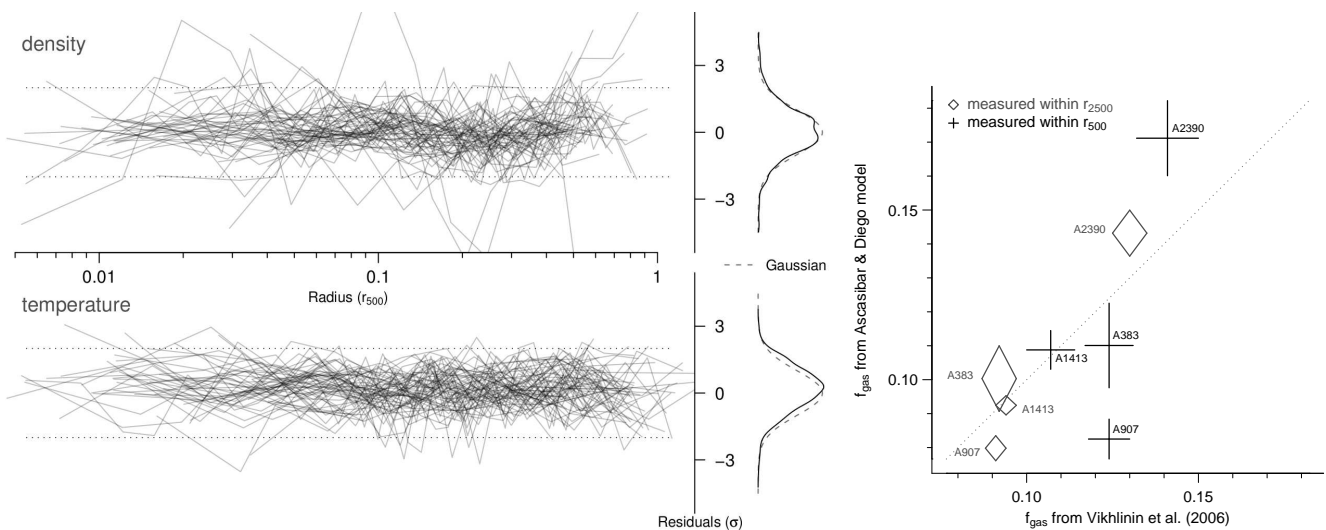


Figure 1. *Left:* A comparison of the residuals from the [Ascasibar & Diego \(2008\)](#) model, normalized by the measurement errors on each point, as a function of scaled radius for both the gas density and temperature data; each line represents a different cluster. Dotted lines mark $\pm 2\sigma$ and the marginal distribution of the data is depicted as a kernel smoothed density estimate, compared to a Gaussian of unit variance. *Right:* A comparison of gas fractions measured within both r_{500} and r_{2500} for the four clusters in common with the sample of [Vikhlinin et al. \(2006\)](#); the dotted line marks the locus of equality.

which, regardless of the ambiguity, the X-ray/BCG projected offset is large.

Each galaxy was classified according to the presence or absence of H α emission lines, as determined from the literature [Crawford et al. \(1999\)](#), Sloan Digital Sky Survey archival spectra ([Adelman-McCarthy et al., 2008](#)) and VLT FORS2 spectra for REFLEX BCGs (PI Edge). For two clusters (Abell 115b and RXC J2211.7-0350) there was no available optical spectrum to determine the emission line status of the BCG. H α emission is a reliable indicator of the presence of central cold material, second only to direct detection of molecular gas at sub-mm wavelengths ([Edge 2001](#)). In addition, we have classified each BCG according to the presence of radio emission detected in the Very Large Array (VLA) FIRST Survey ([Becker, White & Helfand 1995](#)), NVSS ([Condon et al. 1998](#)) and/or SUMSS ([Bock, Large & Sadler 1999](#)) radio surveys. While these three radio surveys have different flux density limits, resolution and frequency, they nevertheless provide a uniform limit of 3 mJy at 1.4 GHz.

3 X-RAY CLUSTER MODELLING

The deprojected gas temperature and density profiles were fitted jointly to the phenomenological cluster model of [Ascasibar & Diego \(2008\)](#), using the χ^2 statistic, in order to determine the gravitating mass profile and parametrize the gas thermodynamic structure ([Sanderson, in preparation](#)). The best-fit cluster model was also used to estimate r_{500} , the radius enclosing a mean overdensity of 500 with respect to the critical density of the Universe at the cluster redshift. Any spectral bins lying within 5 kpc of the centre were excluded from the fit, owing to systematic deviations from the model which are expected to be significant on small scales ([Ascasibar & Diego 2008](#)). For the clusters ZwCl 0839.9+2937 and Abell 1758N it was necessary to exclude the central bins from the fit (lying at 10 and 30 kpc, respectively) due to significant deviations from the best-fit model.

The left panel of Fig. 1 shows the residuals from the model for both the gas temperature and density, as a function of scaled

radius. It is clear that the model provides a good description of the data, with no indication of any significant systematic deviations. The marginal distribution of the residuals is consistent with the Gaussian distribution expected from the measurement errors alone, with only a small shift discernible in the case of the temperature profile—indicating that on average the model tends to slightly ($\sim 0.3\sigma$) underpredict the data. There is particularly good agreement between the data and the model in the gas density at all radii, including $0.04r_{500}$, where we use the logarithmic gradient to quantify the strength of cooling (Section 4.3). It should be noted that the gas density profiles extend only to the penultimate spectral bin, owing to the non-trivial volume element associated with the outermost annulus in the deprojection ([Sanderson et al. 2006](#)).

As an additional test of the model, the right panel of Fig. 1 plots the derived gas fraction (f_{gas}) within both r_{2500} and r_{500} compared to measurements made by [Vikhlinin et al. \(2006\)](#), for the four clusters common to both samples. We calculate errors on f_{gas} and all other derived quantities directly, using the median absolute deviation of 200 bootstrap resamplings of the input temperature and density profile data. There is generally reasonable agreement in f_{gas} , particularly for the measurements within r_{2500} , and no indication of serious systematic trends, although both Abell 907 and Abell 2390 are significant outliers, within r_{500} . This disagreement points to the importance of systematics associated with cluster modelling, for example differences in the number and location of radial bins, as well as the choice of mass profile parametrization. Nevertheless, we emphasize the close match between our cluster model fits and the data, as seen in residuals from the model. Furthermore, in Fig. 7 (Section 4.4) we demonstrate good agreement between r_{500} compared to measurements made by [Maughan et al. \(2008\)](#), where we address the issue of bias in X-ray mass estimates in relation to cluster dynamical state.

4 RESULTS

4.1 X-ray/BCG offset

A number of recent studies have identified the projected separation between the BCG and the *peak* of the cluster X-ray emission as an important parameter in understanding the activity of the BCG, both in terms of star formation (e.g. [Edwards et al. 2007](#); [Bildfell et al. 2008](#); [Cavagnolo et al. 2008](#)) and AGN radio emission (e.g. [Cavagnolo et al. 2008](#); [Mittal et al. 2008](#)). However, while the X-ray peak can accurately identify the focus of a cool core, this location may not always lie at the ‘centre’ of the hot gas, as defined for the purposes of conducting a radial profile analysis. This is particularly true for non-CC clusters, which have much broader and flatter X-ray cores. We therefore investigate the projected offset between the BCG and both the peak and centroid of the X-ray emission. We assess the relative merits of both definitions in the context of quantifying cluster dynamical state in Section 4.3, but turn our attention initially to the projected offset in terms of the centroid.

[Fig. 2](#) shows the distribution of X-ray centroid/BCG projected offsets for the sample, in units of arcseconds, kiloparsecs and r_{500} . The distributions are roughly lognormal, with medians of 13 kpc / 1.0 per cent of r_{500} . Also plotted are the separate distributions for BCGs with and without detected $H\alpha$ line emission, and a clear difference is apparent: the BCGs with line emission all have small projected offsets from the X-ray cluster centroid, within a maximum of 15 kpc / 1.5 per cent of r_{500} . Conversely, BCGs with no detected $H\alpha$ emission lines have preferentially larger X-ray centroid/BCG projected offsets (median values = 35 kpc / 2.8 per cent of r_{500}). This confirms that close proximity of the BCG to the X-ray cluster centroid is a pre-requisite for BCG star formation, in agreement with recent work ([Edwards et al. 2007](#); [Bildfell et al. 2008](#); [Rafferty et al. 2008](#)).

For comparison, [Fig. 3](#) shows the distribution of projected offsets for BCGs with and without detected radio emission. As with the $H\alpha$ emitters in [Fig. 2](#), the clusters with radio detected BCGs have smaller X-ray/BCG offsets. However, a separate peak of radio detected BCGs with intermediate projected offsets is also present. For the sample as a whole, the interquartile range of X-ray/BCG projected offsets is $0.0035\text{--}0.04r_{500}$ (see bottom right panel of [Fig. 5](#)), demonstrating that BCGs in X-ray selected clusters are generally located close to the cluster X-ray centroid; all but two (97^{+2}_{-4} per cent) lie within $0.15r_{500}$.

4.2 BCG $H\alpha$ and radio emission

[Table 1](#) summarizes the $H\alpha$ and radio emission status of the 63 clusters for which both classifications are available. Roughly half the galaxies are passive (30/63), with no detected $H\alpha$ or radio emission. The radio active fraction is 49 ± 7 per cent, which is larger than the value of $\gtrsim 30$ per cent found in clusters selected optically ([Best et al. 2007](#)) and in X-rays ([Lin & Mohr 2007](#)), possibly due to the high average mass of the clusters in the LoCuSS sample. Similarly, the fraction of $H\alpha$ emitting BCGs (37 ± 7 per cent) is somewhat higher than the value of 27 per cent for the X-ray selected cluster sample of [Crawford et al. \(1999\)](#), which is itself roughly double the fraction in optically-selected clusters (13 per cent; [Edwards et al. 2007](#)). A Pearson’s χ^2 test strongly rejects the null hypothesis that the presence or absence of detected $H\alpha$ emission is independent from the presence or absence of radio emission, with a χ^2 value of 25.7 for 1 degree of freedom and a correspond-

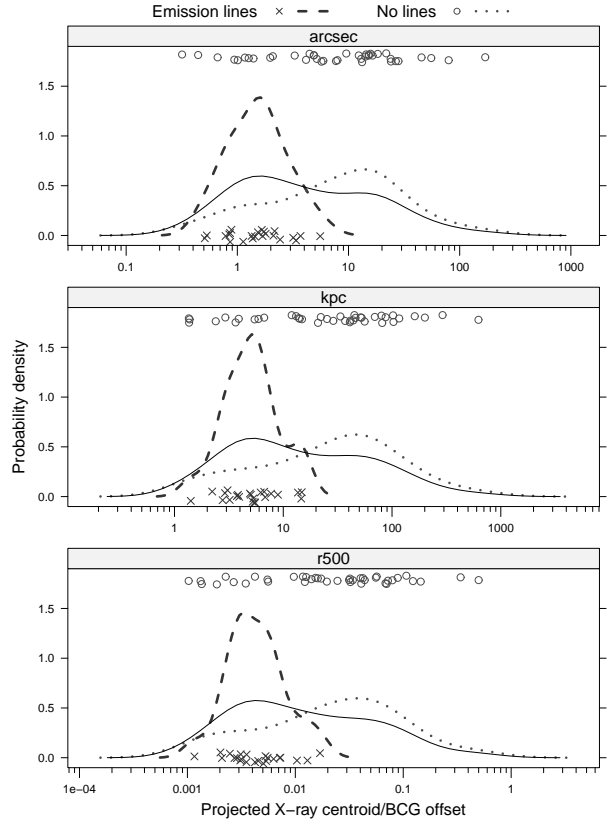


Figure 2. Kernel-smoothed probability density estimates of the distribution of projected offsets between the X-ray cluster centroid and the BCG. The raw values are shown at randomly ‘jittered’ y -axis positions. The distributions for BCGs with and without detected $H\alpha$ emission are also indicated.

	Emission lines	No lines	Sum
Radio emission	21 (0.33)	10 (0.16)	31 (0.51)
No radio	2 (0.03)	30 (0.48)	32 (0.49)
Sum	23 (0.36)	40 (0.64)	63 (1)

Table 1. A contingency table of the BCG distribution according to their $H\alpha$ and radio emission status, with fractions of the total (63) given in brackets. Note that the two clusters with unknown emission line status are excluded.

ing p -value of 4.0×10^{-7} . This demonstrates the close correspondence between BCG activity in terms of star formation and black hole accretion.

4.3 Cluster cool core status

In order to connect the properties of the BCG to those of its host cluster, we focus on the cooling state of the intracluster medium (ICM). A key signature of cool core clusters is a cuspy gas density– and hence surface brightness– profile, which can be more accurately measured than the associated decline in temperature. Furthermore, the gradient of the gas density profile on small scales progressively steepens with increased cooling, even before a significant cool core is established ([Ettori & Brighenti 2008](#)). Therefore, following [Vikhlinin et al. \(2007\)](#), we use the parameter α , defined as the logarithmic slope of the gas density profile at $0.04r_{500}$, to quantify the extent of cluster gas cooling on the approximate scale

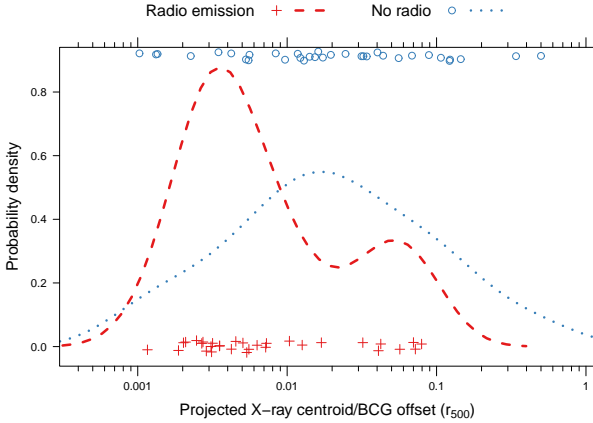


Figure 3. Kernel-smoothed probability density estimates of the distribution of projected X-ray/BCG offsets, normalized to r_{500} . The data are separated according to whether or not radio emission is detected from the BCG and the raw values are shown at randomly ‘jittered’ y -axis positions.

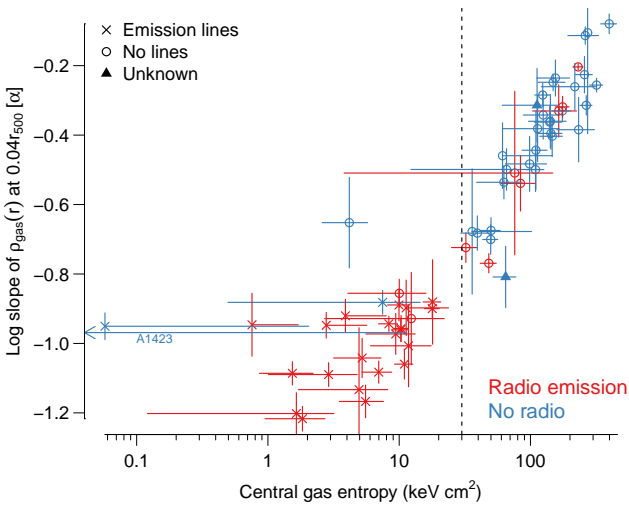


Figure 4. α (see Section 4.3) versus central gas entropy, from the best-fit cluster model. The vertical dashed line marks 30 keV cm^2 . Point styles indicate the presence or absence of $\text{H}\alpha$ emission lines in the BCG and the colour shows whether significant radio emission is detected from the BCG. The zero value for Abell 1423 is plotted as an arrow from its upper bound.

of any central galaxy, with more negative values implying stronger cooling.

We calculate the logarithmic slope, α , from the best-fit [Ascibar & Diego \(2008\)](#) cluster model and plot it, in Fig. 4, against the central gas entropy, which is a direct indicator of the cooling state of the ICM. However, this measurement involves extrapolation of the model to zero radius, unlike α , which is evaluated at a directly accessible radius, which also lies in a region where the model provides a good fit to the density profile (Fig. 1, left panel). The strong correlation in Fig. 4 demonstrates the effectiveness of α as a simple means of quantifying cool-core strength.

It can be seen from Fig. 4 that there is a gap in the entropy values which separates the clusters into two regimes, with all the $\text{H}\alpha$ emitting BCGs lying in clusters with central entropy $< 30 \text{ keV cm}^2$, as discovered by [Rafferty et al. \(2008\)](#) and subsequently confirmed by [Cavagnolo et al. \(2008\)](#). Furthermore, there

are a number of clusters with a central gas entropy of $\sim 10 \text{ keV cm}^2$, with the remainder grouped around $\sim 100\text{--}200 \text{ keV cm}^2$ as also found by [Cavagnolo et al.](#) This threshold entropy level can be understood as being determined by the physics of thermal conduction ([Voit et al. 2008](#)), which can also account for the bifurcation into CC and non-CC populations (e.g. [Guo, Oh & Ruszkowski 2008](#); [Sanderson et al. 2009](#)).

Given the greater ease and reliability with which α can in general be measured, we use this as the parameter of choice for quantifying cool core strength. We now turn to the issue of how cluster cooling is related to the X-ray/BCG offset. Fig. 5 shows the variation of α with X-ray/BCG projected offset (scaled by r_{500}) defined using both the X-ray centroid (left panel) and peak (right panel). A clear trend is evident, with the strongest cooling cores found only in clusters with small projected X-ray/BCG offsets. [Vikhlinin et al. \(2007\)](#) suggest $\alpha < -0.7$ for strong cooling flows, which lies close to the gap in the distribution of values. However, it is clear that only those clusters with $\alpha \lesssim -0.85$ and a projected offset $\lesssim 0.02r_{500}$ have detected $\text{H}\alpha$ line emission (as depicted by the shaded box), which is indicative of genuine gas condensation and subsequent star formation associated with unchecked cooling. Of the 24 systems in this shaded region, only 1 is passive, and 21 have both $\text{H}\alpha$ and radio emission; there are no $\text{H}\alpha$ emitting BCGs outside the shaded region.

While the two panels in Fig. 5 show similar results, the correlation between α and the X-ray *centroid*/BCG projected offset is stronger and shows fewer outliers: the Kendall rank correlation coefficient gives $\tau = 0.48$ (p -value = 1.3×10^{-8}) for the offset with respect to the centroid and $\tau = 0.42$ (p -value = 6.7×10^{-7}) for the peak. Nevertheless, a number of prominent outliers are still present in the left panel of Fig. 5 and are labelled in both panels. In particular Abell S0592 and RXC J0232.2-4420, which have relatively large X-ray/BCG offsets, despite hosting strong cool cores. Abell S0592 has an obvious subclump (excluded from the X-ray analysis) which is associated with the BCG; the main peak X-ray centroid is located close ($< 10 \text{ kpc}$) to another galaxy. RXC J0232.2-4420, on the other hand, has a relatively regular and single-peaked morphology, but with 2 bright galaxies of which the less luminous is located close to ($< 10 \text{ kpc}$) the X-ray centroid.

The only passive cluster with a steep α and small projected X-ray/BCG offset is Abell 1423. While there is an extended radio source very close to the BCG, inspection of the FIRST Survey image indicates that this is an unrelated narrow angle tail radio galaxy seen in projection and that the BCG is undetected to the FIRST depth. No optical lines were detected by [Crawford et al. \(1999\)](#) but the spectrum was not of the highest quality so more detailed follow-up of this BCG would be of great interest. The two remaining labelled points are the clusters RXC J0220.9-3829 and Abell 3088, which are the only other systems in the shaded box with BCGs that have no significant radio emission.

While it is clear that $\text{H}\alpha$ emitting BCGs are all concentrated in the bottom left corner of Fig. 5 (particularly the left panel), the distribution of passive BCGs (blue circles, with no $\text{H}\alpha$ or radio emission) follows a continuous strong trend: a test with the Kendall rank correlation coefficient for the centroid offset case gives a value of $\tau = 0.53$ (p -value = 2.0×10^{-5}) in favour of the null hypothesis that the two quantities are uncorrelated. The equivalent Kendall coefficient for the peak offset case is $\tau = 0.48$ (p -value = 1.0×10^{-3}). This suggests a progressive weakening of central gas cooling with increasing cluster disruption, as measured by the X-ray/BCG projected offset, even for clusters with no evidence of condensation from the hot phase.

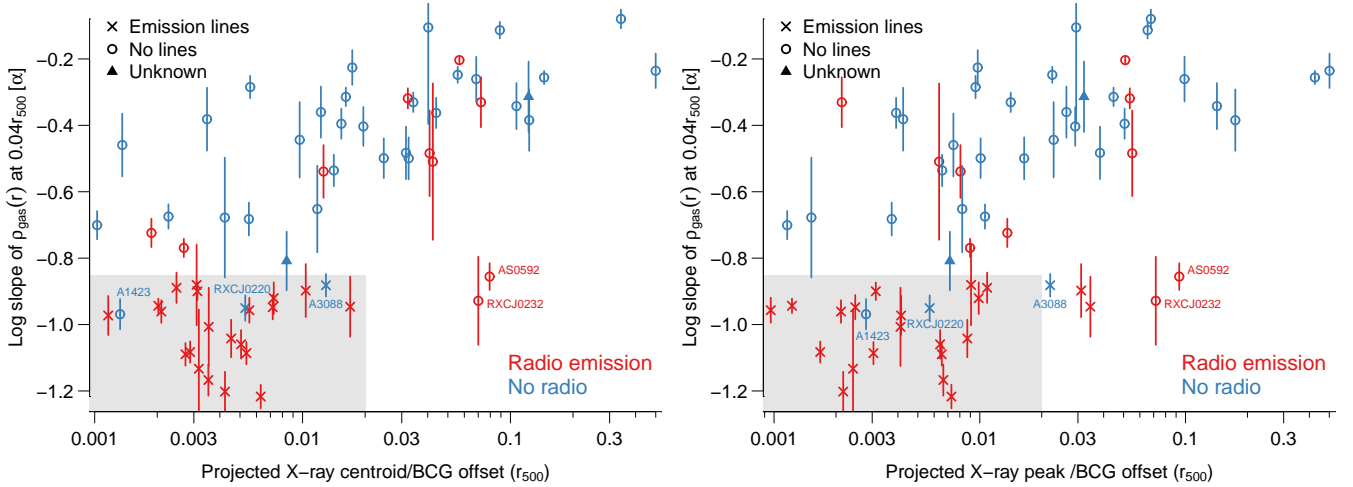


Figure 5. α (see Section 4.3) plotted against the projected offset between the BCG and the X-ray *centroid* (left panel) and the X-ray *peak* (right panel). The shaded box highlights the region occupied by line emitting galaxies in the left panel.

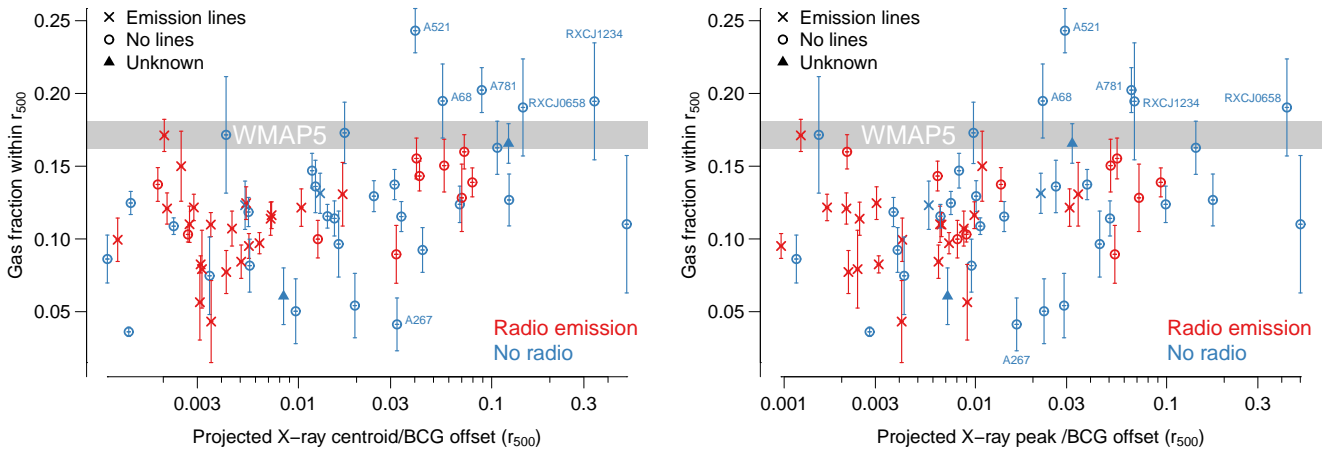


Figure 6. Cluster gas fraction within r_{500} as a function of projected offset between the BCG and the X-ray *centroid* (left panel) and the X-ray *peak* (right panel). The horizontal shaded region depicts the Universal baryon fraction as measured from the five year WMAP data (Dunkley et al. 2009). Outliers identified in Fig. 7 are labelled: see text for details.

4.4 Cluster gas fraction and dynamical state

To explore the connection between X-ray/BCG offset and cluster dynamical state, we plot in Fig. 6 the gas fraction (f_{gas}) within r_{500} as a function of projected X-ray/BCG offset, with the Universal baryon fraction (f_b) from the five year WMAP data (Dunkley et al. 2009) also indicated. As in Fig. 5, the relation is shown for the offset in terms of both the X-ray centroid (left panel) and peak (right panel). A test with the Kendall coefficient for the centroid offset case gives $\tau = 0.31$ (p -value = 3.0×10^{-4}) in favour of the null hypothesis that f_{gas} and the X-ray/BCG offset are uncorrelated. The equivalent Kendall coefficient for the peak offset case is $\tau = 0.24$ (p -value = 5.0×10^{-3}). In contrast, there is no significant correlation between the X-ray/BCG offset and the cluster mean temperature or total mass, which might otherwise account for such a trend with f_{gas} (cf. Sanderson et al. 2003; Vikhlinin et al. 2006)

All of the five clusters statistically consistent with having gas fraction values in excess of the WMAP5 f_b upper bound are passive systems and all have projected X-ray/BCG offsets exceeding $0.03r_{500}$ — all are also identified as outliers in Fig. 7 (see be-

low). The cluster gas fraction within r_{500} is typically ~ 90 per cent of the cosmic mean (e.g. Crain et al. 2007) and the baryon fraction in massive clusters is roughly 10 per cent higher than f_{gas} (e.g. Lin, Mohr & Stanford 2003; Gonzalez, Zaritsky & Zabludoff 2007). Therefore such large gas fractions are unrealistic and may indicate a failure of the assumption of hydrostatic equilibrium in the cluster modelling, as might result from significant dynamical disturbance (Nagai, Vikhlinin & Kravtsov 2007). These objects are therefore likely to be outliers and significant sources of scatter in scaling relations. Taking the nominal X-ray/BCG offset value of $0.02r_{500}$ used to identify the strongest cool core clusters (see Fig. 5), the mean gas fraction of the ‘small offset’ clusters ($\leq 0.02r_{500}$) is 0.106 ± 0.005 ($\sigma = 0.03$) compared to 0.145 ± 0.009 ($\sigma = 0.04$) for the clusters with an offset $> 0.02r_{500}$.

The only emission line BCG cluster with a high gas fraction in Fig. 6 is Abell 2390 ($f_{\text{gas}} = 0.17 \pm 0.01$, lying within the WMAP5 f_b band), which is a hot cluster (9.8 keV) that had the highest f_{gas} in the 13 cluster sample of Vikhlinin et al. (2006) and which is a known merging system, despite hosting a cool core

(Allen, Ettori & Fabian 2001). As pointed out above, the comparison between our f_{gas} value and that of Vikhlinin et al. (Fig. 1, right panel) reveals a clear discrepancy within r_{500} . Nevertheless, the agreement is better within r_{2500} , and our r_{500} value of 1437 ± 68 kpc is very close to the value of 1416 ± 48 kpc calculated by Vikhlinin et al.. Furthermore, it can be seen from inspection of figure 12 in Vikhlinin et al. (2006) that their gas fraction profile for Abell 2390 rises sharply just outside r_{500} , reaching values consistent with our measurement, albeit at a slightly larger radius.

To explore the effectiveness of the projected offset between the BCG and the X-ray centroid in quantifying the cluster dynamical state, we turn to a comparison between r_{500} determined from two different methods. Fig. 7 shows the comparison between r_{500} as calculated from the Ascasisbar & Diego cluster model and that measured by Maughan et al. (2008) using a scaling relation based on the X-ray equivalent to the Compton y -parameter (Y_X ; Kravtsov, Vikhlinin & Nagai 2006). Y_X is simply the total thermal energy of the hot gas within a given radius, and acts as a robust mass proxy, even for dynamically disturbed clusters (Kravtsov et al. 2006; Poole et al. 2007; Maughan 2007). The 30 clusters common to both samples are split into four subsamples defined by quartiles of the projected X-ray centroid/BCG offset. In general, the agreement is excellent, particular for the clusters in the 50th percentile of X-ray centroid/BCG projected offset (top panels of Fig. 7), however six prominent outliers are visible and have been labelled.

The Ascasisbar & Diego cluster model assumes hydrostatic equilibrium (HSE) to derive r_{500} , whereas r_{500} inferred from Y_X is only sensitive to the total thermal energy of the gas. A comparison between the two values therefore reveals the extent to which the assumption of HSE applies for any given cluster. For five of the outliers in Fig. 7 the Ascasisbar & Diego underpredicts r_{500} compared to the Y_X -based measurement of Maughan et al., consistent with the tendency for HSE-based measurements to underestimate the cluster mass (Nagai et al. 2007). These outliers all fall in the highest two quartiles of X-ray centroid/BCG projected offset, further supporting the view that this offset acts as an indicator of dynamical disturbance (cf. Katayama et al. 2003). The remaining cluster, Abell 267, has a complex mass distribution, based on the gravitational lensing analysis of Smith et al. (2005), which has a highly elliptical morphology. This could result in the HSE-based X-ray analysis *overestimating* the total mass, as suggested by the comparison of r_{500} in Fig. 7, as well as its low f_{gas} (0.041 ± 0.018 ; Fig. 6), given its large mass ($M_{500} = 1.85 \pm 0.70 \times 10^{15} M_{\odot}$).

5 SUMMARY AND DISCUSSION

We have shown that the projected X-ray/BCG offset is highly correlated with the strength of cooling in the host cluster core, as measured by the logarithmic slope of the gas density profile at $0.04r_{500}$ (α ; Section 4.3) and that the gas fraction is systematically larger in clusters with large offsets. In particular, the use of the X-ray *centroid* yields a stronger correlation in both these relations, compared to using the X-ray *peak* to calculate this offset.

Our results also demonstrate that the activity of BCGs is closely related to the properties of their host cluster, and specifically the proximity to and strength of any cool core. The behaviour of the H α emitting galaxies is especially striking in that all 23 of them in our sample of 65 BCGs are found close to ($\lesssim 0.02r_{500}$) a strong ($\alpha \lesssim -0.85$; Section 4.3) cool core, with only 1 other non-emission line galaxy meeting these same criteria. This is consistent

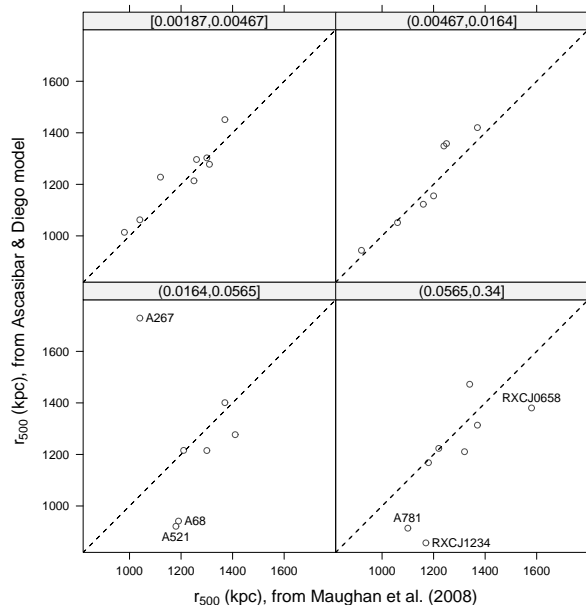


Figure 7. The comparison between r_{500} calculated from the Ascasisbar & Diego (2008) cluster model and that measured by Maughan et al. (2008) for the 30 clusters common to both samples. The clusters have been split into quartiles according to their projected X-ray centroid/BCG offset, increasing from the top left to bottom right, as indicated by the range in the strip for each panel (0.00187–0.00467; 0.00467–0.0164; 0.0164–0.0565; 0.0565–0.34 r_{500}). The dashed lines indicate the locus of equality.

with the work of Rafferty et al. (2008) and Cavagnolo et al. (2008) who find that star formation only occurs once the hot gas entropy falls below a critical threshold of $\sim 30 \text{ keV cm}^2$. Voit et al. (2008) show that such a threshold can be understood if energy output from AGN is coupled to the cooling gas via thermal conduction, a process which is also capable of thermally stabilizing *non-cool* core clusters (Sanderson et al. 2009).

Notwithstanding the effects of conduction or galaxy feedback, it is clear that star formation is ultimately able to take place when the BCG coincides closely with a strong cool core. As a consequence, additional enrichment of the ICM is possible in the vicinity of the BCG, which may explain the centrally peaked metallicity profiles of cool core clusters (Leccardi & Molendi 2008; Sanderson et al. 2009) and the fact that the lowest entropy gas is also the most enriched (Sanderson et al. 2009). The influence of the BCG on the ICM may also account for the increased variation in gas properties (e.g. metallicity and entropy) on small scales ($\sim 0.02r_{500}$; Sanderson et al. 2009).

The strong connection between line emission and radio emission (Section 4.2) suggests that star formation and AGN accretion are fuelled from the same source. However, a significant fraction (23 per cent; 7/31) of the radio emitting BCGs occupy a narrow range of relatively large offsets $0.032\text{--}0.079r_{500}$ and have no H α emission, suggesting a different origin. These may be cases where recent merger disruption has triggered a brief burst of AGN activity.

If the X-ray/BCG projected offset serves to measure the dynamical state of the cluster, with more disturbed systems having larger values, then its strong correlation with the steepness of the gas density profile (α) implies that cool core strength progressively diminishes in more dynamically disrupted clusters. Such a trend

would be expected if cluster mergers were capable of erasing cool cores. There is a notable dearth in Fig. 5 of clusters with relatively flat density profiles and small projected X-ray/BCG offsets. Such cases ought to exist if AGN outbursts alone were capable of reheating cool cores, or if strong preheating prevented their formation altogether (McCarthy et al. 2008). On the other hand, if such processes had a disruptive impact on the core X-ray morphology, then this might shift the centroid as measured on \sim arcmin scales enough to explain the trend.

ACKNOWLEDGMENTS

AJRS thanks Trevor Ponman and Ria Johnson for useful discussions. We thank our colleagues in the LoCuSS collaboration for their encouragement and help, in particular, we thank Eiichi Egami and Victoria Hamilton-Morris for allowing us to use the CTIO data in advance of their publication, and Chris Haines for help with BCG identification. We are grateful to the referee, Ben Maughan, for a prompt response and helpful suggestions which have improved the paper. AJRS and GPS acknowledge support from STFC and GPS acknowledges support from the Royal Society. This work made use of the NASA/IPAC Extragalactic Database (NED).

REFERENCES

- Adelman-McCarthy J. K., et al., 2008, *ApJS*, 175, 297 3
- Allen S. W., Ettori S., Fabian A. C., 2001, *MNRAS*, 324, 877 7
- Ascasibar Y., Diego J. M., 2008, *MNRAS*, 383, 369 3, 5, 7
- Becker R. H., White R. L., Helfand D. J., 1995, *ApJ*, 450, 559 3
- Beers T. C., Flynn K., Gebhardt K., 1990, *AJ*, 100, 32 2
- Best P. N., von der Linden A., Kauffmann G., Heckman T. M., Kaiser C. R., 2007, *MNRAS*, 379, 894 1, 4
- Bildfell C., Hoekstra H., Babul A., Mahdavi A., 2008, *MNRAS*, 389, 1637 1, 4
- Bock D. C.-J., Large M. I., Sadler E. M., 1999, *AJ*, 117, 1578 3
- Cavagnolo K. W., Donahue M., Voit G. M., Sun M., 2008, *ApJ*, 683, L107 1, 4, 5, 7
- Condon J. J., Cotton W. D., Greisen E. W., Yin Q. F., Perley R. A., Taylor G. B., Broderick J. J., 1998, *AJ*, 115, 1693 3
- Crain R. A., Eke V. R., Frenk C. S., Jenkins A., McCarthy I. G., Navarro J. F., Pearce F. R., 2007, *MNRAS*, 377, 41 6
- Crawford C. S., Allen S. W., Ebeling H., Edge A. C., Fabian A. C., 1999, *MNRAS*, 306, 857 1, 3, 4, 5
- Dunkley J., Komatsu E., Nolta M. R., Spergel D. N., Larson D., Hinshaw G., Page L., Bennett C. L., Gold B., Jarosik N., Weiland J. L., Halpern M., Hill R. S., Kogut A., Limon M., Meyer S. S., Tucker G. S., Wollack E., Wright E. L., 2009, *ApJS*, 180, 306 6
- Edge A. C., 1991, *MNRAS*, 250, 103 1
- Edge A. C., 2001, *MNRAS*, 328, 762 3
- Edwards L. O. V., Hudson M. J., Balogh M. L., Smith R. J., 2007, *MNRAS*, 379, 100 1, 4
- Ettori S., Brighenti F., 2008, *MNRAS*, 387, 631 4
- Gonzalez A. H., Zaritsky D., Zabludoff A. I., 2007, *ApJ*, 666, 147 6
- Guo F., Oh S. P., Ruszkowski M., 2008, *ApJ*, 688, 859 5
- Heckman T. M., 1981, *ApJ*, 250, L59 1
- Katayama H., Hayashida K., Takahara F., Fujita Y., 2003, *ApJ*, 585, 687 1, 7
- Kravtsov A. V., Vikhlinin A., Nagai D., 2006, *ApJ*, 650, 128 7
- Leccardi A., Molendi S., 2008, *A&A*, 487, 461 7
- Lin Y., Mohr J. J., Stanford S. A., 2003, *ApJ*, 591, 749 6
- Lin Y.-T., Mohr J. J., 2004, *ApJ*, 617, 879 1
- Lin Y.-T., Mohr J. J., 2007, *ApJS*, 170, 71 4
- Maughan B. J., 2007, *ApJ*, 668, 772 7
- Maughan B. J., Jones C., Forman W., Van Speybroeck L., 2008, *ApJS*, 174, 117 2, 3, 7
- McCarthy I. G., Babul A., Bower R. G., Balogh M. L., 2008, *MNRAS*, 386, 1309 8
- Mittal R., Hudson D. S., Reiprich T. H., Clarke T., 2008, *A&A*, accepted (arXiv:0810.0797) 1, 4
- Nagai D., Vikhlinin A., Kravtsov A. V., 2007, *ApJ*, 655, 98 6, 7
- Okabe N., Takada M., Umetsu K., Futamase T., Smith G. P., 2009, *PASJ*, submitted (arXiv:0903.1103) 2
- Peres C. B., Fabian A. C., Edge A. C., Allen S. W., Johnstone R. M., White D. A., 1998, *MNRAS*, 298, 416 1
- Poole G. B., Babul A., McCarthy I. G., Fardal M. A., Bildfell C. J., Quinn T., Mahdavi A., 2007, *MNRAS*, 380, 437 7
- Rafferty D. A., McNamara B. R., Nulsen P. E. J., 2008, *ApJ*, 687, 899 1, 4, 5, 7
- Sanderson A. J. R., O’Sullivan E., Ponman T. J., 2009, *MNRAS*, 395, 764 2, 5, 7
- Sanderson A. J. R., Ponman T. J., Finoguenov A., Lloyd-Davies E. J., Markevitch M., 2003, *MNRAS*, 340, 989 6
- Sanderson A. J. R., Ponman T. J., O’Sullivan E., 2006, *MNRAS*, 372, 1496 2, 3
- Smith G. P., Kneib J.-P., Smail I., Mazzotta P., Ebeling H., Czoske O., 2005, *MNRAS*, 359, 417 1, 7
- Stott J. P., Edge A. C., Smith G. P., Swinbank A. M., Ebeling H., 2008, *MNRAS*, 384, 1502 2
- Sun M., Voit G. M., Donahue M., Jones C., Forman W., Vikhlinin A., 2009, *ApJ*, 693, 1142 2
- Vikhlinin A., Burenin R., Forman W. R., Jones C., Hornstrup A., Murray S. S., Quintana H., 2007, in Böhringer H., Pratt G. W., Finoguenov A., Schuecker P., eds, *Heating versus Cooling in Galaxies and Clusters of Galaxies Lack of Cooling Flow Clusters at $z > 0.5$* . p. 48 4, 5
- Vikhlinin A., Kravtsov A., Forman W., Jones C., Markevitch M., Murray S. S., Van Speybroeck L., 2006, *ApJ*, 640, 691 3, 6, 7
- Vikhlinin A., McNamara B. R., Forman W., Jones C., Quintana H., Hornstrup A., 1998, *ApJ*, 502, 558 2
- Voit G. M., Cavagnolo K. W., Donahue M., Rafferty D. A., McNamara B. R., Nulsen P. E. J., 2008, *ApJ*, 681, L5 1, 5, 7
- Zhang Y.-Y., Finoguenov A., Böhringer H., Kneib J.-P., Smith G. P., Kneissl R., Okabe N., Dahle H., 2008, *A&A*, 482, 451 2